

HERMES: CURRENT COSMIC INFRARED BACKGROUND ESTIMATES ARE CONSISTENT WITH
CORRELATED EMISSION FROM KNOWN GALAXIES AT $z < 4^\dagger$ M.P. VIERO^{1,2}, L. MONCELSI², R.F. QUADRI³, M. BÉTHERMIN^{4,5}, J. BOCK^{2,6}, D. BURGARELLA⁷, S.C. CHAPMAN⁸,
D.L. CLEMENTS⁹, A. CONLEY¹⁰, L. CONVERSI¹¹, S. DUVENVOORDEN¹², J.S. DUNLOP¹³, D. FARRAH¹⁴, A. FRANCESCHINI¹⁵,
R.J. IVISON^{16,13}, G. LAGACHE⁷, G. MAGDIS¹⁷, L. MARCHETTI¹⁵, J. ÁLVAREZ-MÁRQUEZ⁷, G. MARSDEN¹⁸, S.J. OLIVER¹²,
M.J. PAGE¹⁹, I. PÉREZ-FOURNON^{20,21}, B. SCHULZ^{2,22}, DOUGLAS SCOTT¹⁸, I. VALTCHANOV¹¹, J.D. VIEIRA^{23,24}, L. WANG^{25,26},
J. WARDLOW²⁷, M. ZEMCOV^{2,6}

Draft version March 10, 2019

ABSTRACT

We report contributions to cosmic infrared background (CIB) intensities originating from known galaxies, and their companions, at submillimeter wavelengths. Using the publicly-available UltraVISTA catalog, and maps at 250, 350, and 500 μm from *Herschel*/SPIRE, we perform a novel measurement that exploits the fact that correlated sources will bias stacked flux densities if the resolution of the image is poor; i.e., we intentionally smooth the image — in effect degrading the angular resolution — before stacking and summing intensities. By smoothing the maps we are capturing the contribution of faint (undetected in $K_S \sim 23.4$) sources that are physically associated with the detected sources. We find that the cumulative CIB increases with increased smoothing, reaching 9.82 ± 0.78 , 5.77 ± 0.43 , and $2.32 \pm 0.19 \text{ nWm}^{-2}\text{sr}^{-1}$ at 250, 350, and 500 μm at 300 arcsec full width half maximum. This corresponds to a fraction of the fiducial CIB of 0.94 ± 0.23 , 1.07 ± 0.31 , and 0.97 ± 0.26 at 250, 350, and 500 μm , where the uncertainties are dominated by those of the absolute CIB. We then propose, with a simple model combining parametric descriptions for stacked flux densities and stellar mass functions, that emission from galaxies with $\log(M/M_\odot) > 8.5$ can account for the entire measured total intensities, and argue against contributions from extended, diffuse emission. Finally, we discuss prospects for future survey instruments to improve the estimates of the absolute CIB levels, and observe any potentially remaining emission at $z > 4$.

Subject headings: cosmology: observations, submillimeter: galaxies – infrared: galaxies – galaxies: evolution – large-scale structure of universe

1. INTRODUCTION

Since the cosmic infrared background (CIB; Hauser & Dwek 2001) was first detected spectroscopically (Puget et al. 1996) with the Far Infrared Absolute Spectrophotometer (FIRAS; Mather et al. 1999), astronomers have been working to fully understand its origin. Long before its discovery, model predictions argued for a diffuse background in the far-infrared arising from dust-reprocessed photons in distant star-forming ‘primeval galaxies’ (e.g., Partridge & Peebles 1967;

versity of Oxford, Keble Road, Oxford OX1 3RH, UK

¹⁸ Department of Physics & Astronomy, University of British Columbia, 6224 Agricultural Road, Vancouver, BC V6T 1Z1, Canada

¹⁹ Mullard Space Science Laboratory, University College London, Holmbury St. Mary, Dorking, Surrey RH5 6NT, UK

²⁰ Instituto de Astrofísica de Canarias (IAC), E-38200 La Laguna, Tenerife, Spain

²¹ Departamento de Astrofísica, Universidad de La Laguna (ULL), E-38205 La Laguna, Tenerife, Spain

²² Infrared Processing and Analysis Center, MS 100-22, California Institute of Technology, JPL, Pasadena, CA 91125

²³ Department of Physics, University of Illinois Urbana-Champaign, 1110 W. Green Street, Urbana, IL 61801

²⁴ Astronomy Department, University of Illinois at Urbana-Champaign, 1002 W. Green Street, Urbana, IL 61801

²⁵ SRON Netherlands Institute for Space Research, Landlevan 12, 9747 AD, Groningen, Netherlands

²⁶ Institute for Computational Cosmology, Department of Physics, University of Durham, South Road, Durham, DH1 3LE, UK

²⁷ Dark Cosmology Centre, Niels Bohr Institute, University of Copenhagen, Juliane Maries Vej 30, 2100 Copenhagen, Denmark

¹ Kavli Institute for Particle Astrophysics and Cosmology, Stanford University, 382 Via Pueblo Mall, Stanford, CA 94305; email: marco.viero@stanford.edu

² California Institute of Technology, 1200 E. California Blvd., Pasadena, CA 91125

³ George P. and Cynthia Woods Mitchell Institute for Fundamental Physics and Astronomy, Department of Physics and Astronomy, Texas A&M University, College Station, TX 77843

⁴ Laboratoire AIM-Paris-Saclay, CEA/DSM/Irfu - CNRS - Université Paris Diderot, CE-Saclay, pt courrier 131, F-91191 Gif-sur-Yvette, France

⁵ Institut d’Astrophysique Spatiale (IAS), bâtiment 121, Université Paris-Sud 11 and CNRS (UMR 8617), 91405 Orsay, France

⁶ Jet Propulsion Laboratory, 4800 Oak Grove Drive, Pasadena, CA 91109

⁷ Laboratoire d’Astrophysique de Marseille - LAM, Université d’Aix-Marseille & CNRS, UMR7326, 38 rue F. Joliot-Curie, 13388 Marseille Cedex 13, France

⁸ Dalhousie University, Department of Physics and Atmospheric Science, Coburg Road, Halifax, NS B3H 1A6, Canada

⁹ Astrophysics Group, Imperial College London, Blackett Laboratory, Prince Consort Road, London SW7 2AZ, UK

¹⁰ Center for Astrophysics and Space Astronomy 389-UCB, University of Colorado, Boulder, CO 80309

¹¹ Herschel Science Centre, European Space Astronomy Centre, Villanueva de la Cañada, 28691 Madrid, Spain

¹² Astronomy Centre, Dept. of Physics & Astronomy, University of Sussex, Brighton BN1 9QH, UK

¹³ Institute for Astronomy, University of Edinburgh, Royal Observatory, Blackford Hill, Edinburgh EH9 3HJ, UK

¹⁴ Department of Physics, Virginia Tech, Blacksburg, VA 24061

¹⁵ Dipartimento di Astronomia, Università di Padova, vicolo Osservatorio, 3, 35122 Padova, Italy

¹⁶ UK Astronomy Technology Centre, Royal Observatory, Blackford Hill, Edinburgh EH9 3HJ, UK

¹⁷ Department of Astrophysics, Denys Wilkinson Building, Uni-

Bond, Carr, & Hogan 1986).

Subsequent observations of local starburst galaxies with the *Infrared Astronomical Satellite* (IRAS; Soifer et al. 1984) showed that galaxies could emit a surprisingly large part of their energy in the far-infrared, and ground-based measurements later confirmed the existence of a rare population of extremely luminous submillimeter galaxies (or SMGs; Blain et al. 2002). While these bright objects generated tremendous excitement, and in fact constitute a significant fraction of the total star-formation rate density at $z > 3$ (e.g., Le Floc’h et al. 2005; Murphy et al. 2011), their low abundance only accounts for a small fraction of the total CIB.

The arrival of the *Herschel Space Observatory* — whose instruments, PACS (70, 100, and 160 μm ; Poglitsch et al. 2010) and SPIRE (250, 350, and 500 μm ; Griffin et al. 2010), bracket the peak of the thermal spectrum of dust emission — brought the promise of directly detecting less luminous and far more numerous dusty star-forming galaxies (DSFGs). However, source confusion resulting from the relatively large point-spread functions (e.g., Nguyen et al. 2010) limited the number of galaxies that could be individually resolved by PACS at 100 and 160 μm to 58% and 74% of the CIB, respectively, (Berta et al. 2011), and by SPIRE at 250 μm to 15% (Oliver et al. 2012). Statistical methods including stacking (e.g., Béthermin et al. 2012; Viero et al. 2013a) and $P(D)$ (Glenn et al. 2010; Berta et al. 2011) performed better, resolving 89% and 70% of the CIB at 100 and 250 μm , respectively.

The origin of the rest remained unclear. Viero et al. (2013a) suggested that the missing flux could be tied up in faint sources — faint either because they are low mass, at high redshift, or extremely dusty. Another possible source is diffuse emission from the dust that is known to be distributed in the halos of galaxies (Ménard et al. 2010; Hildebrandt et al. 2013), and could be heated by stripped stars (e.g., Tal & van Dokkum 2011; Zemcov et al. 2014).

Here we present a technique to demonstrate that most, if not all, of the CIB can be accounted for by galaxies detected in current near-infrared surveys ($K_S \approx 23.4$) and objects correlated with them, at $z < 4$. We show with a simple model that galaxies alone are the most plausible source of this signal, without any need for extended emission or other exotic sources, and argue that any remaining CIB likely originates from galaxies at still higher redshifts.

2. DATA

2.1. UltraVISTA Catalog

We perform our analysis on catalogs and images located in the COSMOS (Scoville et al. 2007) field, centered at $10^{\text{h}}00^{\text{m}}26^{\text{s}}, +2^{\circ}13'00''$. We use the $K_S = 23.4$ (AB)-selected, publicly-available¹ catalog from Muzzin et al. (2013b, UltraVISTA), which consists of a 1.62 deg^2 subset of the full COSMOS field, where both near-infrared and optical wavelengths are available (30 bands in all). The catalog contains photometric redshifts computed with EAZY (Brammer et al. 2008), and

stellar-masses computed with FAST (Kriek et al. 2009). Galaxies are split into star-forming or quiescent based on their positions in the rest-frame $U - V$ vs. $V - J$ color-color diagram (UVJ ; Williams et al. 2009). Following Viero et al. (2013a), we split the sample into 8×8 bins of redshift ($z = 0$ to 4 with $\Delta z = 0.5$) and stellar mass (5 star-forming and 3 quiescent bins).

2.2. Herschel/HerMES Submillimeter Maps

We use submillimeter maps observed with the Spectral and Photometric Imaging REceiver (SPIRE; Griffin et al. 2010) at 250, 350, and 500 μm from the Herschel Multi-tiered Extragalactic Survey (HerMES; Oliver et al. 2012). COSMOS is a level 5 field, consisting of 4 repeat observations, to an instrumental depth of 15.9, 13.3, and 19.1 mJy (5σ), with confusion adding an additional noise term of 24.0, 27.5, and 30.5 mJy (5σ) at 250, 350, and 500 μm , respectively (Nguyen et al. 2010). Absolute calibration is detailed in Griffin et al. (2013), with calibration uncertainties of 5%. Maps are custom made with 4 arcsec pixels at all wavelengths using the SMAP (Levenson et al. 2010; Viero et al. 2013b) pipeline.

SPIRE maps are chosen specifically for this study because SPIRE is particularly sensitive to the CIB, since its wavelengths probe the rest-frame peak of thermal dust emission at $z = 1-3$ (Madau & Dickinson 2014), and because large-scale features can be reconstructed with minimal filtering (Pascale et al. 2011).

3. METHOD

As was first demonstrated explicitly by Marsden et al. (2009), ‘stacking’ in its simplest form is nothing more than the covariance (or zero-lag cross-correlation) of a catalog with a mean-subtracted map. They further showed with simulations that stacking on positions drawn from an uncorrelated catalog (i.e., one without any clustering) in a mean-subtracted map will *always* result in an unbiased estimate, regardless of the angular resolution of the instrumental point-spread function (PSF, or beam). Realistically, of course, all catalog objects (in a given redshift interval) are clustered at some level, and that will lead to biased estimates if simple stacking is applied without corrections (e.g., Serjeant et al. 2008; Fernandez-Conde et al. 2010).

Many methods exist to account for biases due to correlations, most of which generally fall into two categories: those that fit a clustering profile to the excess flux due to clustering in a stacked thumbnail (e.g., Béthermin et al. 2012; Heinis et al. 2013); and those that use the catalog to construct synthetic images that are then fit to the original image (e.g., Kurczynski & Gawiser 2010; Viero et al. 2013a). Determining the effects of clustering of the catalog objects themselves is relatively simple; the insidious thing is the clustering of catalog sources with other, uncatalogued, submillimeter emitters. If there are correlated sources in the image that are missing from the catalog, their combined flux will bias the estimate. And because the level of the bias depends on the angular resolution of the image, stacking with a larger beam is more susceptible to bias from missing sources.

Here we demonstrate an image-fitting method to determine the extent to which correlated sources, both known and unknown, contribute to the CIB. We do this by ex-

¹ <http://www.strw.leidenuniv.nl/galaxyevolution/ULTRAVISTA>

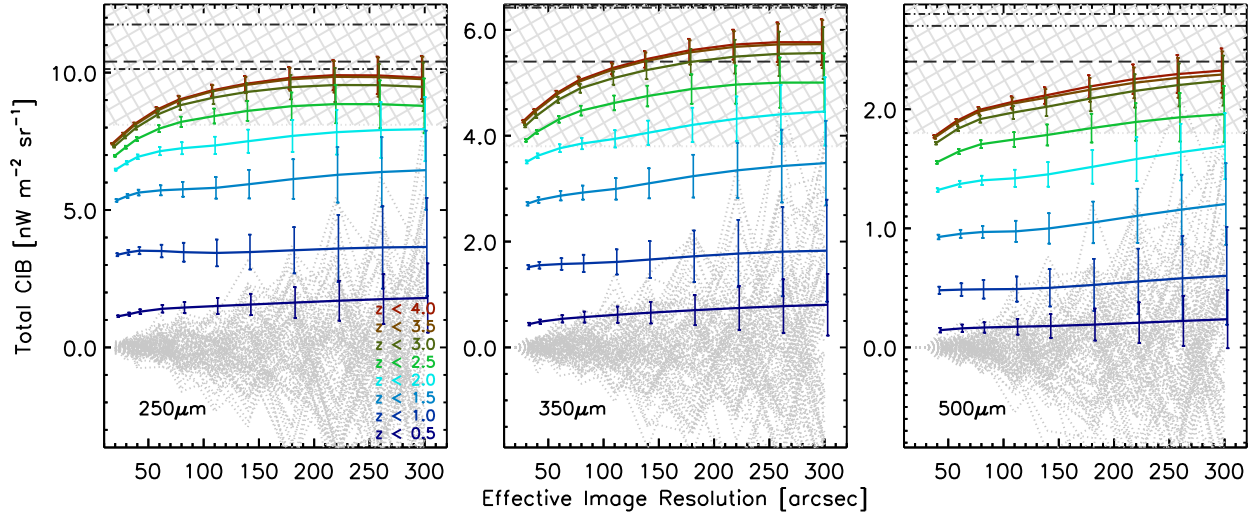


FIG. 1.— Cumulative measured CIB vs. the size of the effective image resolution (in arcsec, FWHM) at 250 (left panel), 350 (center panel), and 500 μm (right panel). The Fixsen et al. (1998) FIRAS values are shown as dashed lines with gray hatched regions, while the Lagache et al. (1999) FIRAS values are shown as 3-dot-dashed lines, and the Béthermin et al. (2012) model estimates are shown as dot-dashed lines. Colors represent the sum over all bins up to the given z . Grey dotted lines show the full set of null tests for the $z < 4$ case. The cumulative CIB vs. effective resolution increases more rapidly at higher redshift, where the catalog is increasingly incomplete. The flattening of the curve at the highest redshift suggests that any potential remaining intensity lies at higher redshifts. Tabulated values can be found at <https://web.stanford.edu/~viero/downloads.html>.

exploiting the property that larger beams result in larger biases and artificially degrade the angular resolution of the image by convolving the maps with Gaussians; any correlated emission in the sky that is missing from the catalog is absorbed as a bias in the sources being measured. Emission that is not correlated — say, emission coming from sources at redshifts greater than those of our catalog objects — will not influence the primary measurement, except as a potential noise term.

3.1. SIMSTACK

For this analysis we use the publicly-available SIMSTACK code², which is described in detail in Viero et al. (2013a). SIMSTACK falls into the category of image fitting rather than thumbnail stacking. Briefly, synthetic images of the sky are constructed from correlated subsets of catalogs (i.e., objects in the same redshift range) with the assumption that galaxies that are physically similar — in this case quiescent or star-forming galaxies within a stellar mass bin — have comparable infrared luminosities and submillimeter flux densities. Synthetic images are then convolved with the PSF of the instrument, and are fit simultaneously to the actual sky map to retrieve the mean flux densities of the subsample.

We smooth the maps and synthetic images by convolving them with Gaussians of width $\sigma_{\text{smooth}} = \sqrt{\sigma_{\text{eff}}^2 - \sigma_{\text{SPIRE}}^2}$, i.e., the geometric difference of the nominal SPIRE and effective beams, where the nominal SPIRE resolutions are 17.5, 23.7, and 34.6 arcsec at 250, 350, and 500 μm , respectively, and the effective resolutions are 20, 30, 40, 60, 80, 110, 140, 180, 220, 260, and 300 arcsec. Above 300 arcsec, statistical uncertainties overwhelm the measurement (see Section 4.1). The reported effective resolutions are chosen to be spaced closer where the changes in cumulative CIB are larger.

All synthetic images and sky maps are mean-subtracted before stacking.

Stacking is performed separately for each set of synthetic images and maps. Stacked flux densities are then color-corrected to account for the observed spectral shape of the sources through the passbands, with temperatures taken from Viero et al. (2013a, Equation 18). Color corrections range between, 1.006–0.984, 0.993–0.977, and 1.007–0.991 at 250, 350, and 500 μm , respectively.

We use simulations to check that stacking and smoothing with a Gaussian, as opposed to the measured SPIRE beam or any other kernel, is a reasonable approximation, with bias of less than 4% for the largest smoothing kernel, which we include in the reported errors. We test that the method does not introduce biases by performing 100 null tests for each set of synthetic images and maps. Null tests involve running the identical stacking pipeline with the same binning of sources, but after randomizing the positions of the sources in the catalogs. Because the map and images are mean-subtracted, we expect the stacked flux densities of the null tests to be consistent with zero. In Section 4.1 we show that this is the case.

We note that this method has the advantage that missing sources are not double-counted, meaning that the flux density from a single missing object will be distributed among the synthetic images, rather than appearing multiple times (as would be the case in thumbnail stacking). Also note that stacked flux densities are intentionally *not* corrected for completeness because it is precisely the flux densities of the missing (i.e., incomplete, but similarly applies to misclassified AGN or DSFGs) sources that we are attempting to measure by degrading the effective resolution of the map. As a result, this technique is not limited to CIB studies, but is applicable to any study where estimates of the level of faint, correlated emission are in question.

² <https://www.stanford.edu/~viero/downloads.html>

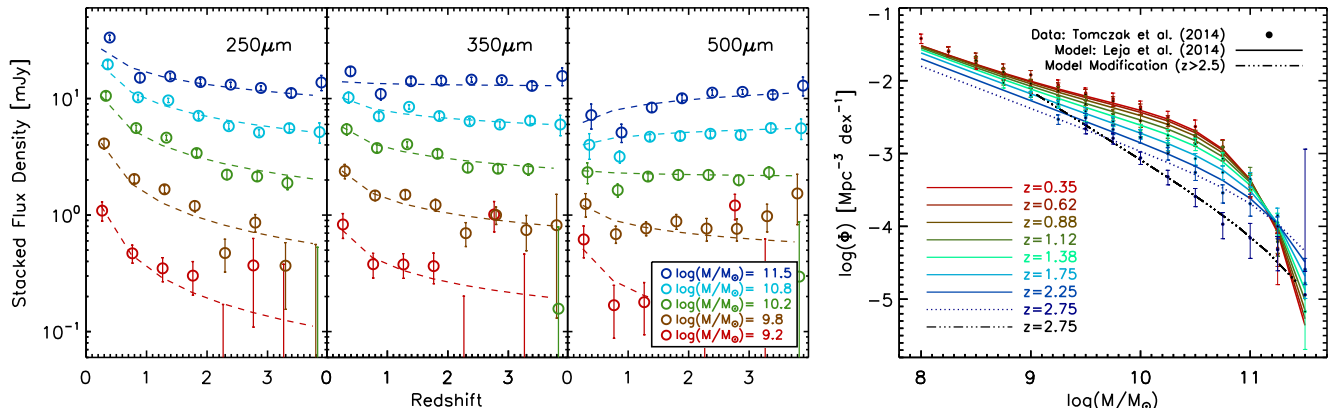


FIG. 2.— Left three panels: Stacked flux densities (measured with nominal PSFs) in divisions of stellar-mass vs. redshift for star-forming galaxies. Power-law model fits (described in Section 5.1) are shown as dotted lines. Right panel: Parametric model for the stellar mass functions of star-forming galaxies adopted from Leja et al. (2015). The dotted line is where the model diverges from the measured mass functions of e.g., Tomczak et al. (2014) and Muzzin et al. (2013a); the dot-dashed line illustrates the modified model determined at $z > 2.5$ by interpolating between the Leja et al. (2015) model and the Muzzin et al. (2013a) data.

4. RESULTS

4.1. Cumulative CIB

We report total intensities of our stacking measurement as the cumulative sum over redshift (from $z = 0$ to the redshifts labeled with different color lines) vs. the effective resolution of the image, in Figure 1³. At lower redshifts ($z < 1$) the fractional CIB that is measured increases weakly with increasing effective beam size, which is expected given that the completeness of the catalog at these redshifts is near unity for stellar masses $\log(M/M_\odot) \geq 9$. Conversely, at higher redshifts the fractional CIB that is measured increases rapidly with increased smoothing. The maximum CIB we resolve is 9.82 ± 0.78 , 5.77 ± 0.43 , 2.32 ± 0.19 nWm⁻²sr⁻¹ at 250, 350, and 500 μ m.

Estimates of the exact measured fraction of the absolute CIB are limited by the uncertainties in the reported absolute values of the CIB derived from FIRAS spectra by Fixsen et al. (1998) and Lagache et al. (1999), which range between 22% and 30%. The Fixsen et al. (1998) levels (10.4 ± 2.3 , 5.4 ± 1.6 , 2.6 ± 0.6 ; hereafter chosen to represent the fiducial values) are shown as dashed lines in Figure 1, and the Lagache et al. (1999) levels (11.8 ± 2.9 , 6.4 ± 1.6 , 2.7 ± 0.7) are shown as 3-dot-dashed lines. Additionally, Béthermin et al. (2012, dot-dashed lines) provide an estimate of the total CIB by extrapolating their measured source counts, finding they agreed with FIRAS, but with similarly large uncertainties. In total we find that the fraction of the fiducial CIB we resolve is 0.94 ± 0.23 , 1.07 ± 0.31 , and 0.97 ± 0.26 at 250, 350, and 500 μ m, respectively.

The full set of 100 null tests at each effective beam size for $z < 4$ are shown as gray dotted lines in Figure 1. As expected, the results of the null tests fluctuate around zero, with the magnitude of that fluctuation increasing with increasing effective beam size. Additional systematic uncertainties include calibration and beam area uncertainties, and cosmic variance, which is estimated following Moster et al. (2011).

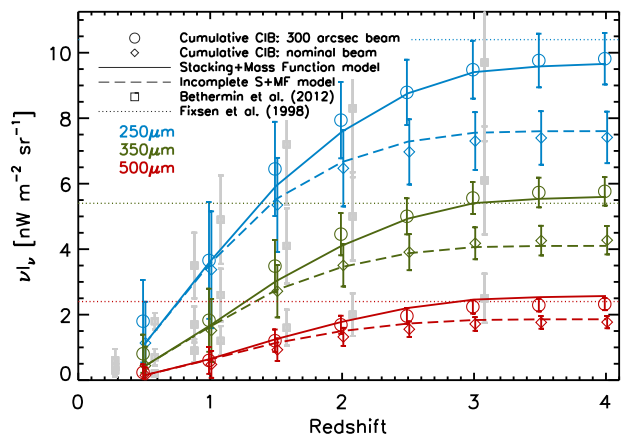


FIG. 3.— Measurements (open circles) and models (solid lines) for cumulative CIB intensities vs. redshift. Measurements are the cumulative sums for images stacked at the highest effective beam size of 300". The models, described in Section 5.1, combine parametric descriptions for the stacked flux densities (at the native resolution of the images) and the stellar mass functions (see Figure 2). Extrapolated counts from Béthermin et al. (2012) are shown as gray squares. Also shown are cumulative CIB intensities vs. redshift on stacks made with the native (i.e., non-smoothed) SPIRE images (diamonds), and the models after they have been modified to match the incompleteness of the actual catalog (dashed lines).

5. DISCUSSION

It is interesting to consider the nature of the undetected sources that are captured by our smoothing procedure: are they very low-mass galaxies; massive but dusty galaxies that evade detection in current deep K -selected catalogs; or some other unknown component?

We now propose — through a simple model that combines a parametric description of the stellar mass function with simple fits to nominal stacked flux densities — that the galaxies that make up the stellar mass function are alone able to describe our measurement, and that by extension the missing CIB originates from galaxies in the low-mass end of the stellar mass function.

³ Tabulated values for the intensities in Figure 1 can be found at <https://web.stanford.edu/~viero/downloads.html>

5.1. A Model of the CIB

The first component of the model adopts the Leja et al. (2015, Equation 1) parameterization of the Tomczak et al. (2014) stellar mass function. The right-most panel of Figure 2 illustrates the performance of the Leja et al. (2015) model against the Tomczak et al. (2014) data. We find that it diverges from the measurements at higher redshifts and so we add a modification at $z > 2.5$ by simply interpolating between the model and the measured stellar mass functions of Muzzin et al. (2013a) to $z = 4$.

Similarly, the second component of the model consists of power-law fits to the stacked flux densities vs. lookback time for each stellar mass bin, with the added condition that the mass dependence of the slopes and offsets themselves follow smooth functions. The three left panels of Figure 2 show the stacked flux densities and best-fit power laws as open circles with error bars, and dotted lines, respectively. Finally, the model is integrated over the redshift range $z = 0.1\text{--}4$, and stellar mass range $\log(M/M_\odot) = 8\text{--}14$; although the contribution from galaxies below $\log(M/M_\odot) < 8.5$ is found to be negligible.

Figure 3 compares the resulting model (solid lines) with the full CIB measurements (open circles) at all three wavelengths. The Béthermin et al. (2012, shown in the Figure as gray squares) estimates, derived by extrapolating number counts, are in good agreement. We note some tension with the Planck Collaboration et al. (2014) intensity at $350\text{ }\mu\text{m}$ ($7.7 \pm 0.2\text{ nWm}^{-2}$), which is an output of the halo model that is fit to CIB power spectra; although their $550\text{ }\mu\text{m}$ estimate from the same model is in relative agreement ($2.3 \pm 0.1\text{ nWm}^{-2}$).

Also shown (as diamonds) are measurements made when stacking on the native SPIRE images (i.e., no smoothing), and are again compared to the model (dashed lines), but this time *the model is modified to match the completeness values of the actual catalog*. The fit is again remarkable, and is a testament to the completeness estimates of the catalog.

Arguments for additional, diffuse, sources of CIB; in particular dust in the extended halos of galaxies (Ménard et al. 2010), are disfavored by our model.

5.2. A CIB beyond z of 4?

While our measurements are consistent with the fiducial levels of the total CIB, the existing uncertainties on the absolute level are so large that it is difficult to convincingly estimate how much CIB is still unresolved. Any missing CIB is more likely to occur at longer wavelengths, which are more sensitive to higher redshifts (because of the negative K -correction; Blain et al. 2003), from where we would expect uncorrelated emission to originate.

Indeed, several exceptional ULIRG-like galaxies have been identified at $z > 4$, albeit with low abundances (e.g., Riechers et al. 2013; Vieira et al. 2013; Dowell et al. 2014; Swinbank et al. 2014). However, basic extrapolations of the contribution of ULIRGs to the star-formation rate density at $z > 4$ (e.g., Murphy et al. 2011; Viero et al. 2013a) points to them dominating the far-infrared emission at this epoch. Determining the relative levels that they and less luminous galaxies contribute is a key question going forward.

To resolve these high- z questions, more data are required; particularly: i) an update of the absolute CIB; ii) deeper catalogs with stellar masses and redshifts to redshifts greater than 4; iii) submillimeter surveys (350 to $1000\text{ }\mu\text{m}$) with large angular-scale fidelity and smaller PSFs in the regions of those deep catalogs — particularly at longer wavelengths which are more sensitive to galaxies at higher redshifts. The former can only be achieved with space-based missions to measure the DC level above atmospheric foregrounds. The second requirement is steadily growing from multiple current or upcoming efforts (e.g., SDSS/BOSS, CANDLES, DES, LSST), although the photometric redshifts for very dusty galaxies may remain quite uncertain (see Spitler et al. 2014). The last point will require a ground-based submillimeter observatory similar in scope to CCAT (Sebring et al. 2006).

6. CONCLUSION

We find that most of the CIB at SPIRE wavelengths (250 , 350 , and $500\text{ }\mu\text{m}$) can be accounted for by galaxies detected in current near-infrared surveys of moderate depth ($K_S \approx 23.4$), and the galaxies correlated with them. We report total intensities of 9.82 ± 0.78 , 5.77 ± 0.43 , $2.32 \pm 0.19\text{ nWm}^{-2}\text{sr}^{-1}$ at 250 , 350 , and $500\text{ }\mu\text{m}$, which corresponds to a fraction of the fiducial absolute CIB of 0.94 ± 0.23 , 1.07 ± 0.31 , and 0.97 ± 0.26 .

We find that a simple model combining parametric descriptions for the stellar mass function and stacked flux densities for $\log(M/M_\odot) > 8.5$ and $z < 4$ is able to convincingly reproduce the measurements, and argues against a significant contribution from diffuse emission such as intergalactic dust. We note that emission from objects that are not in the catalog, *and* is either uncorrelated with catalog objects or exists at scales greater than 300 arcsec , would be missed. However unlikely, this cannot be ruled out without a better absolute measurement to compare against.

Finally, we propose that any remaining CIB likely originates from galaxies at $z > 4$, and if so should be detectable at submillimeter and millimeter wavelengths.

ACKNOWLEDGMENTS

MPV warmly thanks Charlotte Clarke, Pete Hurley, Seb Oliver, and the University of Sussex for their hospitality during the development of this study; and Phil Hopkins for valuable discussions of the $z > 4$ Universe. SPIRE has been developed by a consortium of institutes led by Cardiff Univ. (UK) and including: Univ. Lethbridge (Canada); NAOC (China); CEA, LAM (France); IFSI, Univ. Padua (Italy); IAC (Spain); Stockholm Observatory (Sweden); Imperial College London, RAL, UCL-MSSL, UKATC, Univ. Sussex (UK); and Caltech, JPL, NHSC, Univ. Colorado (USA). This development has been supported by national funding agencies: CSA (Canada); NAOC (China); CEA, CNES, CNRS (France); ASI (Italy); MCINN (Spain); SNSB (Sweden); STFC, UKSA (UK); and NASA (USA). The SPIRE data for this paper were obtained as a part of proposal KPGT_soliver_1, with images made using the following OBSIDs: 1342222819-26, 1342222846-54, 1342222879-80, 1342222897-901.

REFERENCES

- Berta, S., Magnelli, B., Nordon, R., Lutz, D., Wuyts, S., Altieri, B., Andreani, P., Aussel, H., et al. 2011, *A&A*, 532, A49
- B  thermin, M., Le Floch, E., Ilbert, O., Conley, A., Lagache, G., Amblard, A., Arumugam, V., Aussel, H., et al. 2012, *A&A*, 542, A58
- Blain, A. W., Barnard, V. E., & Chapman, S. C. 2003, *MNRAS*, 338, 733
- Blain, A. W., Smail, I., Ivison, R. J., Kneib, J.-P., & Frayer, D. T. 2002, *Phys. Rep.*, 369, 111
- Bond, J. R., Carr, B. J., & Hogan, C. J. 1986, *ApJ*, 306, 428
- Brammer, G. B., van Dokkum, P. G., & Coppi, P. 2008, *ApJ*, 686, 1503
- Dowell, C. D., Conley, A., Glenn, J., Arumugam, V., Asboth, V., Aussel, H., Bertoldi, F., B  thermin, M., et al. 2014, *ApJ*, 780, 75
- Fernandez-Conde, N., Lagache, G., Puget, J.-L., & Dole, H. 2010, *A&A*, 515, A48
- Fixsen, D. J., Dwek, E., Mather, J. C., Bennett, C. L., & Shafer, R. A. 1998, *ApJ*, 508, 123
- Glenn, J., Conley, A., B  thermin, M., Altieri, B., Amblard, A., Arumugam, V., Aussel, H., Babbedge, T., et al. 2010, *MNRAS*, 409, 109
- Griffin, M. J., Abergel, A., Abreu, A., Ade, P. A. R., Andr  , P., Augeres, J.-L., Babbedge, T., Bae, Y., et al. 2010, *A&A*, 518, L3
- Griffin, M. J., North, C. E., Schulz, B., Amaral-Rogers, A., Bendo, G., Bock, J., Conversi, L., Conley, A., et al. 2013, *MNRAS*, 434, 992
- Hauser, M. G. & Dwek, E. 2001, *ARA&A*, 39, 249
- Heinis, S., Buat, V., B  thermin, M., Aussel, H., Bock, J., Boselli, A., Burgarella, D., Conley, A., et al. 2013, *MNRAS*, 429, 1113
- Hildebrandt, H., van Waerbeke, L., Scott, D., B  thermin, M., Bock, J., Clements, D., Conley, A., Cooray, A., et al. 2013, *MNRAS*, 429, 3230
- Kriek, M., van Dokkum, P. G., Labb  , I., Franx, M., Illingworth, G. D., Marchesini, D., & Quadri, R. F. 2009, *ApJ*, 700, 221
- Kurczynski, P. & Gawiser, E. 2010, *AJ*, 139, 1592
- Lagache, G., Abergel, A., Boulanger, F., D  sert, F. X., & Puget, J.-L. 1999, *A&A*, 344, 322
- Le Floch, E., Papovich, C., Dole, H., Bell, E. F., Lagache, G., Rieke, G. H., Egami, E., P  rez-Gonz  lez, P. G., et al. 2005, *ApJ*, 632, 169
- Leja, J., van Dokkum, P. G., Franx, M., & Whitaker, K. E. 2015, *ApJ*, 798, 115
- Levenson, L., Marsden, G., Zemcov, M., Amblard, A., Blain, A., Bock, J., Chapin, E., Conley, A., et al. 2010, *MNRAS*, 409, 83
- Madau, P. & Dickinson, M. 2014, *ARA&A*, 52, 415
- Marsden, G., Ade, P. A. R., Bock, J. J., Chapin, E. L., Devlin, M. J., Dicker, S. R., Griffin, M., Gundersen, J. O., et al. 2009, *ApJ*, 707, 1729
- Mather, J. C., Fixsen, D. J., Shafer, R. A., Mosier, C., & Wilkinson, D. T. 1999, *ApJ*, 512, 511
- M  nard, B., Scranton, R., Fukugita, M., & Richards, G. 2010, *MNRAS*, 405, 1025
- Moster, B. P., Somerville, R. S., Newman, J. A., & Rix, H.-W. 2011, *ApJ*, 731, 113
- Murphy, E. J., Chary, R.-R., Dickinson, M., Pope, A., Frayer, D. T., & Lin, L. 2011, *ApJ*, 732, 126
- Muzzin, A., Marchesini, D., Stefanon, M., Franx, M., McCracken, H. J., Milvang-Jensen, B., Dunlop, J. S., Fynbo, J. P. U., et al. 2013a, *ApJ*, 777, 18
- Muzzin, A., Marchesini, D., Stefanon, M., Franx, M., Milvang-Jensen, B., Dunlop, J. S., Fynbo, J. P. U., Brammer, G., et al. 2013b, *ApJS*, 206, 8
- Nguyen, H. T., Schulz, B., Levenson, L., Amblard, A., Arumugam, V., Aussel, H., Babbedge, T., Blain, A., et al. 2010, *A&A*, 518, L5+
- Oliver, S. J., Bock, J., Altieri, B., Amblard, A., Arumugam, V., Aussel, H., Babbedge, T., Beelen, A., et al. 2012, *MNRAS*, 424, 1614
- Partridge, R. B. & Peebles, P. J. E. 1967, *ApJ*, 148, 377
- Pascale, E., Auld, R., Dariush, A., Dunne, L., Eales, S., Maddox, S., Panuzzo, P., Pohlen, M., et al. 2011, *MNRAS*, 415, 911
- Planck Collaboration, Ade, P. A. R., Aghanim, N., Armitage-Caplan, C., Arnaud, M., Ashdown, M., Atrio-Barandela, F., Aumont, J., et al. 2014, *A&A*, 571, A30
- Poglitich, A., Waelkens, C., Geis, N., Feuchtgruber, H., Vandenbussche, B., Rodriguez, L., Krause, O., Renotte, E., et al. 2010, *A&A*, 518, L2
- Puget, J.-L., Abergel, A., Bernard, J.-P., Boulanger, F., Burton, W. B., Desert, F.-X., & Hartmann, D. 1996, *A&A*, 308, L5+
- Riechers, D. A., Bradford, C. M., Clements, D. L., Dowell, C. D., P  rez-Fournon, I., Ivison, R. J., Bridge, C., Conley, A., et al. 2013, *Nature*, 496, 329
- Scoville, N., Aussel, H., Brusa, M., Capak, P., Carollo, C. M., Elvis, M., Gialalisco, M., Guzzo, L., et al. 2007, *ApJS*, 172, 1
- Sebring, T. A., Giovanelli, R., Radford, S., & Zmuidzinas, J. 2006, in *Society of Photo-Optical Instrumentation Engineers (SPIE) Conference Series*, Vol. 6267, Society of Photo-Optical Instrumentation Engineers (SPIE) Conference Series, 2
- Serjeant, S., Dye, S., Mortier, A., Peacock, J., Egami, E., Cirasuolo, M., Rieke, G., Borys, C., et al. 2008, *MNRAS*, 386, 1907
- Soifer, B. T., Rowan-Robinson, M., Houck, J. R., de Jong, T., Neugebauer, G., Aumann, H. H., Beichman, C. A., Boggess, N., et al. 1984, *ApJ*, 278, L71
- Spitler, L. R., Straatman, C. M. S., Labb  , I., Glazebrook, K., Tran, K.-V. H., Kacprzak, G. G., Quadri, R. F., Papovich, C., et al. 2014, *ApJ*, 787, L36
- Swinbank, A. M., Simpson, J. M., Smail, I., Harrison, C. M., Hodge, J. A., Karim, A., Walter, F., Alexander, D. M., et al. 2014, *MNRAS*, 438, 1267
- Tal, T. & van Dokkum, P. G. 2011, *ApJ*, 731, 89
- Tomczak, A. R., Quadri, R. F., Tran, K.-V. H., Labb  , I., Straatman, C. M. S., Papovich, C., Glazebrook, K., Allen, R., et al. 2014, *ApJ*, 783, 85
- Vieira, J. D., Marrone, D. P., Chapman, S. C., De Breuck, C., Hezaveh, Y. D., Wei  , A., Aguirre, J. E., Aird, K. A., et al. 2013, *Nature*, 495, 344
- Viero, M. P., Monceli, L., Quadri, R. F., Arumugam, V., Assef, R. J., B  thermin, M., Bock, J., Bridge, C., et al. 2013a, *ApJ*, 779, 32
- Viero, M. P., Wang, L., Zemcov, M., Addison, G., Amblard, A., Arumugam, V., Aussel, H., B  thermin, M., et al. 2013b, *ApJ*, 772, 77
- Williams, R. J., Quadri, R. F., Franx, M., van Dokkum, P., & Labb  , I. 2009, *ApJ*, 691, 1879
- Zemcov, M., Smidt, J., Arai, T., Bock, J., Cooray, A., Gong, Y., Kim, M. G., Korngut, P., et al. 2014, *Science*, 346, 732